Acta Crystallographica Section B
Structural Science
ISSN 0108-7681

First (3 + 2)-dimensional superspace approach to the structure of levyclaudite-(Sb), a member of the cylindrite-type minerals

Michel Evain,[a]* Vaclav Petricek,[b] Yves Moëlo[a] and Colette Maurel[c]‡

[a]Laboratoire de Chimie des Solides, IMN, UMR 6502 CNRS, Université de Nantes, 2 rue de la Houssinière, BP 32229, 44322 Nantes CEDEX 3, France, [b]Institute of Physics, Academy of Sciences of the Czech Republic, Na Slovance 2, 182 21 Praha 8, Czech Republic, and [c]CNRS, 1A rue de la Férollerie, 45071 Orléans CEDEX 2, France

‡ Retired.

Correspondence e-mail: michel.evain@cnrs-imn.fr

Received 10 April 2006
Accepted 3 July 2006

The structure of synthetic levyclaudite-(Sb), approximately $(Pb_{1-y}Sb_yS)_{1.357}[Sn_{1-x}(Cu_2)_xS_2]$, has been determined by single-crystal X-ray diffraction on the basis of the (3 + 2)-dimensional superspace approach. This misfit-layer compound, of the cylindrite type, results from the combination of two heavily modulated triclinic Q and H subsystems with a common **q** wavevector and only one shared reciprocal axis (stacking direction). The Q pseudo-tetragonal layer, $\sim(Pb_{0.70}Sb_{0.30}S)$, derived from the NaCl archetype, is positively charged; the H pseudo-hexagonal layer, $\sim(Sn_{0.85}Cu_{0.30}S_2)$, derived from the CdI_2 archetype, is negatively charged, owing to the replacement of Sn^{4+} in an octahedral coordination by Cu^+ pairs in an opposite triangular coordination. The analysis shows a strong transverse displacive modulation of the two layers, referred to as a 'mondulation', correlated to a maximal Sb site occupation factor in the concavity of the Q layer undulation. The wavelength control of the 'mondulation' obeys the vernier principle ($14c_Q \cong 13c_H$), which would correspond to an energy minimization through a charge transfer density modulation wave, common to all two-dimensional misfit-layer inorganic compounds.

1. Introduction

So-called 'two-dimensional misfits' correspond to complex layered crystal structures of the composite type, in which there is the regular alternation of two types of layers, having one or two of their in-plane parameters in an incommensurate ratio (Wiegers & Meerschaut, 1992). The first general overview of this family of compounds, essentially taking into account mineral sulfides and hydroxysulfides, was given by Makovicky & Hyde (1981, completed in 1992). At the end of the eighties numerous synthetic two-dimensional misfits of the chalcogenide type were described, leading to a special volume devoted to 'incommensurate sandwiched layered compounds' (Meerschaut, 1992). During the last decade, many new two-dimensional misfit chalcogenides have been characterized and a new family of complex cobalt oxides of this two-dimensional misfit type was established (Leligny *et al.*, 1999; Lambert *et al.*, 2001).

Although minerals were the first known representatives of two-dimensional misfits, their recognition as non-commensurate structures was very late. For instance, cannizzarite, $Pb_8Bi_{10}S_{23}$, was defined by Zambonini *et al.* (1925); Graham *et al.* (1953) identified in this mineral the close association of two sets of unit cells, like those in a syntactic intergrowth. Matzat (1979) finally solved its composite layered crystal structure on the basis of a long-distance approximation (semi-commensu-

Table 1
Analysis† of the members of the cylindrite–levyclaudite series (cationic ratios on the basis of S = 3356 at).

Synthesis	No.	Cu	Fe	Pb	Sn	Bi	Sb	Pb + Sb + Bi = Q	Q/1.356	Sn + Fe + Cu/2 = H	Q/H
Cyl-FeSb	5	0	0.199	0.772	0.890	0	0.470	1.242	0.916	1.090	1.140
(Cylindrite)	6	0	0.215	0.915	0.801	0	0.432	1.347	0.993	1.016	1.325
	19	0	0.204	0.984	0.790	0	0.383	1.367	1.008	0.993	1.376
	23	0	0.186	1.060	0.714	0	0.488	1.549	1.142	0.899	1.722‡
Cyl-FeBi	22	0	0.175	0.984	0.774	0.389	0	1.374	1.013	0.949	1.447
Cyl-(Cu,Fe)Bi	21	0.242	0.065	1.011	0.808	0.400	0	1.412	1.041	0.993	1.422
Cyl-CuBi	30	0.315	0	0.984	0.861	0.345	0	1.329	0.980	1.019	1.304
(Levyclaudite)	32	0.367	0	0.765	0.830	0.497	0	1.262	0.931	1.014	1.245
	10	0.418	0	0.942	0.801	0.416	0	1.359	1.002	1.010	1.345
	8	0.394	0	1.031	0.812	0.327	0	1.359	1.002	1.009	1.347
	28	0.403	0	0.922	0.776	0.474	0	1.397	1.030	0.978	1.428
	3	0.380	0	0.953	0.779	0.394	0	1.347	0.993	0.969	1.390
	11	0.320	0	1.043	0.799	0.313	0	1.356	1.000	0.959	1.414
	9	0.427	0	0.962	0.732	0.439	0	1.401	1.033	0.945	1.482
Cyl-Cu(BiSb)	2	0.358	0	0.980	0.788	0.188	0.161	1.329	0.980	0.967	1.374
	1	0.369	0	0.984	0.756	0.298	0.081	1.363	1.005	0.941	1.448
Cyl-(Cu,Fe)Sb	7	0.159	0.094	1.007	0.801	0	0.387	1.394	1.028	0.974	1.431
Cyl-CuSb	33	0.324	0	0.920	0.877	0	0.376	1.295	0.955	1.039	1.246
	29	0.340	0	0.955	0.850	0	0.367	1.322	0.975	1.020	1.296
	15	0.380	0	1.016	0.828	0	0.336	1.352	0.997	1.018	1.328
	31	0.300	0	0.996	0.866	0	0.324	1.319	0.973	1.016	1.299
	13	0.342	0	1.047	0.808	0	0.291	1.338	0.987	0.979	1.367
	4	0.336	0	0.984	0.803	0	0.349	1.333	0.983	0.971	1.373
	16	0.311	0	1.054	0.810	0	0.282	1.336	0.985	0.965	1.384
	14§	0.400(5)	0	0.996(9)	0.761(5)	0	0.331(3)	1.326	0.978(12)	0.961(8)	1.38(3)

† S.u. values specified only for the sample used in the structure determination (#14). For all analyses, the maximal relative errors (in %) are 1.3 (Cu); 3.5 (Fe); 1.4 (Pb); 1.0 (Sn); 2.1 (Bi); 0.9 (Sb); 0.6 (S). ‡ Possibly a mixture. § Sample used for the structure determination.

rate model). Cylindrite, $FePb_3Sn_4Sb_2S_{14}$, discovered a long time ago in Bolivia (Frenzel, 1893), forms cylindrical single crystals up to a few centimetres in length and a few millimetres in diameter. Despite the size of these crystals, it was recognized as a two-dimensional misfit only in 1971 by Makovicky, who proposed a first structural model (Makovicky, 1971, 1974*a*), leaving some uncertainties about the cation partitioning between the two constitutive layers.

All two-dimensional misfits of the chalcogenide (or oxide) type are a combination of a pseudo-quadratic layer (labelled Q) with a pseudo-hexagonal one (labelled H; Makovicky & Hyde, 1981). The Q layer is a (100) slab of the PbS/NaCl archetype, two to four atoms thick (for instance 2 in cylindrite, 4 in franckeite); the H layer is more variable, corresponding either to a CdI_2-type layer (one-octahedron thick – for instance cylindrite – or a double CdI_2-type layer, with a van der Waals gap), a tetradymite-type layer (*i.e.* two-octahedra thick, as in cannizzarite) or an NbS_2-type layer (with the cations in a triangular prismatic coordination, one, two or three layers thick and van der Waals gaps between H layers in the multiple layer cases).

The relative orientation of the two Q and H layers depends upon the relative sizes of their constitutive cations. Cylindrite represents the most complex crystal architecture; the *a* axis is given as the stacking direction, when (b_Q, b_H) and (c_Q, c_H) represent the intralayer parameter pairs; b_Q and b_H are in an incommensurate ratio, while c_Q and c_H are generally in a semicommensurate match according to the vernier principle [coincidence of $(n + 1)c_Q$ with nc_H, with n an integer, here from 10 to 15]. Sometimes there is a small relative rotation of the two layers (Wang & Kuo, 1991; Makovicky & Hyde, 1992), so that b_Q and b_H, and c_Q and c_H as a consequence, are no longer parallel.

The chemistry of natural cylindrite is also complex; it necessarily contains Pb, Sb, Sn and Fe as cations, with S as the anion. The Q layer bears all Pb along with the main part of trivalent Sb, and divalent Sn, when present; its formula is $(Pb^{2+}, Sb^{3+}, Sn^{2+} \ldots)S^{2-}$. The H layer bears all tetravalent Sn along with the main part of Fe (in the divalent state) and trivalent Sb; its formula is $(Sn^{4+}, Fe^{2+}, Sb^{3+} \ldots)S^{2-}{}_2$. Owing to the incommensurability, the structural formula of cylindrite is $[(Pb, Sb, Sn \ldots)S]_x{\cdot}[(Sn, Fe, Sb \ldots)S_2]$, with $x \simeq 1.38$. As the Q layer has a cation/S ratio equal to one, the partial substitution of trivalent Sb for divalent Pb (and eventually divalent Sn or Fe) gives an excess of positive charges. Symmetrically, the partial replacement in the H layer, with a cation/S ratio equal to $\frac{1}{2}$, of tetravalent Sn by divalent Fe and trivalent Sb induces a deficit of positive charges, which balances the positive charge of the Q layer. As in all two-dimensional misfits, the stability of the composite structure is thus governed by the inter-layer charge transfer (Makovicky, 1974*b*; Moëlo *et al.*, 1995; Meerschaut *et al.*, 2000).

Levyclaudite, ~$Cu_3Pb_8Sn_7(Bi,Sb)_3S_{28}$, is a natural chemical derivative of cylindrite (Moëlo *et al.*, 1990), obtained when Bi substitutes for Sb, and monovalent Cu for divalent Fe in a 2:1 ratio [it could be called 'cylindrite-(Bi/Cu)']. Syntheses allowed exploration of these two solid solutions (Maurel *et al.*, 1990), but detailed results have not been previously published. The present study is focused on the single-crystal study of a synthetic Sb-pure levyclaudite ['cylindrite-(Sb/Cu)'], using the (3 + 2)-dimensional superspace approach (van Smaalen, 1992, 1995), along with the prior presentation of experimental results.

2. Syntheses within the cylindrite–levyclaudite solid solution

Dry syntheses were carried out in evacuated glass tubes with either the elements or simple sulfides as reactants, in ratios corresponding to possible theoretical compositions within the cylindrite–levyclaudite series, using the approximated stoichiometric formulae from minerals (see Table 1) as a standard. A small excess of sulfur was, however, introduced, to preclude the presence of divalent tin. Temperatures were set at 873 K over 25–72 d. There were 25 runs: 18 with Cu only, 5 with Fe only, and 2 with Cu and Fe. In parallel, there were 12 runs with Sb only, 11 with Bi only, and 2 with Bi and Sb. No run was performed combining Cu with Fe and Bi with Sb.

The major part of the final product was found as massive blocks at the bottom of the tube, but numerous fibres or laths were generally developed on the inner wall, especially at the top of the tube; some isolated crystals reached a few millimetres in length, for a few tenths of a millimetre in width. For each run, the massive product was, on the one hand, partly used for X-ray powder diffraction data (XPD) and, on the other hand, mounted in epoxy as a polished section for electron probe microanalysis (EPM) equipped with a wavelength-dispersive spectrometer (WDS: CAMEBAX SX50 apparatus).

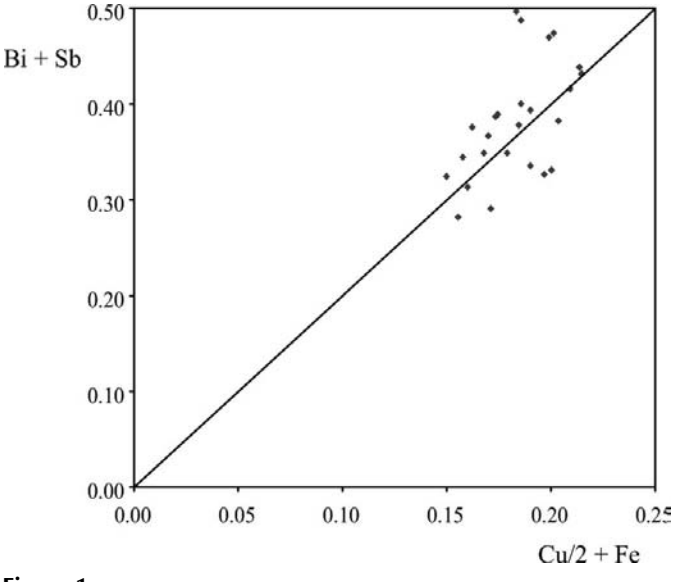

Figure 1
Linear correlation between (Bi + Sb) and (Cu/2 + Fe) visualizing the charge transfer between the two layers (straight line running through the origin and set with a theoretical gradient of 2). Data from Table 1.

In all runs, XPD as well EPM data showed the formation of a member of the cylindrite–levyclaudite 'isomorphous' series as the main constituent, with minor amounts of $PbSnS_3$ (suredaite), and, only in the Bi-rich runs, PbS (galena), CuS (covellite), Cu_2SnS_3 (mohite), $CuPbBiS_3$ (aikinite) or $Pb_6Bi_2S_9$ (heyrovskyite). Table 1 gives the results of EPM analysis (cationic ratios) on the basis of S = 3.356 atoms, as a first approximation. Owing to the two-dimensional misfit character of these compounds, it is worth noticing that the $1 + \delta$ coefficient in $(Pb_ySb_{1-y}S)_{1+\delta}[Sn_x(Cu_2)_{1-x}S_2]$ varies with the chemical composition and that the S total varies, therefore, around the value of 3.356 at.

These syntheses allowed the easy formation of cylindrite (Sb/Fe pole) and levyclaudite (Bi/Cu pole), and also that of the Sb/Cu ['levyclaudite-(Sb)'] and Bi/Fe ['cylindrite-(Bi)'] poles, as well as (two) intermediate compositions between Bi/Cu and Bi/Fe poles, and between Sb/Cu and Sb/Fe poles. The detailed results in Table 1 prove a complete double solid solution according to the substitutions $Sb^{3+} \Leftrightarrow Bi^{3+}$ and $Fe^{2+} \Leftrightarrow 2Cu^{+}$. Fig. 1 represents these analyses as a function of [(Cu/2) + Fe] *versus* (Bi + Sb), in general accordance with the interlayer charge transfer, which requires a distribution of analytical values around a straight line with a gradient of 2 and going through the axis origin. Indeed, to respect the valence balance, the substitution of one Sn^{4+} ion in the H layer by one Fe^{2+} or two Cu^{+} must be compensated by the substitution of two Pb^{2+} by two $(Bi, Sb)^{3+}$ in the Q layer. Fig. 2 illustrates the variable degree of substitution of the major cations (Pb and Sn) for the minor ones, assuming the charge transfer which in this case requires a data distribution that fits with a straight line with a gradient of −1 as a first approximation, according to the substitution rules given above.

While there are numerous EPM data on the cylindrite series, crystallographic data are scarce owing to its structural complexity. The only precise unit cell data were obtained by Makovicky (1976) by X-ray single-crystal diffraction (Table 2), while all other data, generally partial, were acquired through HRTEM (Williams & Hyde, 1988; Wang & Kuo, 1991).

Among the various experimental runs, the synthesis 'LC14' was performed from the pure chemical elements Cu, Pb, Sb, Sn and S in a ratio corresponding to a mixture of levyclaudite-(Sb) ('$Cu_3Pb_8Sb_3Sn_7S_{28}$') with minor bournonite ($CuPbSbS_3$) and a small sulfur excess. Such a starting composition favoured the highest substitution of Sb and Cu for Pb and Sn, respectively, that is, the highest interlayer charge transfer. It gave well crystallized fibres and laths of levyclaudite-(Sb), together with a mass of product at the bottom of the glass tube. Electron microprobe analysis of this product gave the following composition (wt %): Cu 5.3, Pb 42.8, Sb 8.4, Sn 18.8, S 22.3, total 97.6 wt %. On the basis of S = 3.356 at., according to the crystallographic study (see below), the chemical formula $(Pb_{0.996\,(9)}Sb_{0.331\,(3)})(Sn_{0.761\,(5)}Cu_{0.400\,(5)})S_{3.356\,(18)}$, or $(Pb_{0.735}Sb_{0.244}S)_{1.356}\cdot[Sn_{0.766}(Cu_2)_{0.200}]S_2$ is obtained, which has been taken as a first basis for the cation partitioning among the two sub-layers.

Table 2
Unit (sub-) cell data on cylindrite, levyclaudite and levyclaudite-(Sb).

		a (Å)†	b (Å)†	c (Å)†	α (°)†	β (°)†	γ (°)†	c_H/c_Q
Cylindrite	Q sub-cell	11.733 (5)	5.790 (8)	5.810 (5)	90.0 (2)	92.38 20)	93.87 (20)	1.0878
Poopo (Bolivia; Makovicky, 1976)	H sub-cell	11.709 (5)	3.670 (8)	6.320 (5)	90.0 (2)	92.58 (20)	90.85 (20)	$\sim$ 12/11 = 1.0909
Levyclaudite	Q sub-cell	11.84 (1)	5.825 (10)	5.831 (10)	90	92.6 (2)	90	1.0821
Kirkii (Greece; Moëlo *et al.*, 1990)	H sub-cell	11.84 (1)	3.67 (1)	6.31 (1)	90	92.6 (2)	90	$\sim$ 13/12 = 1.0833
Levyclaudite-(Sb)	Q sub-cell	12.1443 (13)	5.8218 (6)	5.8645 (5)	90.019 (8)	92.327 (7)	78.533 (9)	1.0766
Synth. This study	H sub-cell	11.9028 (10)	3.6661 (3)	6.3138 (5)	89.986 (8)	92.490 (7)	90.590 (8)	$\sim$ 14/13 = 1.0769
		c (Å)‡	a (Å)‡	b (Å)‡	γ (°)‡	α (°)‡	β (°)‡	b_H/b_Q

† Setting used in the literature for cylindrite/levyclaudite. ‡ Setting used for the inorganic misfit compound and levyclaudite in this study.

3. Structure determination

3.1. Data collection and data reduction

A platelet of 'LC14' with the dimensions 0.0024 × 0.2 × 0.3 mm^3 was selected and mounted at the tip of a Lindemann capillary by means of a solvent-free glue. The intensity measurement was carried out at room temperature on a Bruker–Nonius KappaCCD diffractometer, using graphite-monochromated Mo K-$L_{2,3}$ radiation (λ = 0.71073 Å). The detector was set at 80 mm for a good resolution and a triclinic mode was selected in the EvalCCD data collection scheme for a full coverage of the diffraction sphere since the standard procedure, using a preliminary cell determined from a frame set, could not be applied. The three-dimensional positions of hundreds of reflections were determined for the diffraction pattern interpretation. A thorough analysis of the reflection distribution then revealed the two misfit subsystem cell orientations: the overall pattern can be interpreted as the combination of two heavily (*i.e.* with satellites up to high order) modulated triclinic subsystems with a common **q** wavevector and only one shared reciprocal axis. It thus resembled the $(SbS)_{1.15}TiS_2$ misfit compound (Ren *et al.*, 1995), but within a configuration that was not predicted by Wiegers *et al.* (1990) in their possible combinations of the intralayer axes (see Fig. 3 and discussion below) and with a much shorter **q** wavevector. As is often the case in misfit-layer compounds, the $a^*_{13} = a^*_{23}$ (c^*) axis of $(SbS)_{1.15}TiS_2$ was chosen as the stacking direction in Ren's structure report. As mentioned in §1, this is not what has been used so far in the cylindrite–levyclaudite series for which the a^* axis was chosen as the characteristic direction (Makovicky & Hyde, 1992). However, to be consistent with all previous structure reports on misfit compounds, we prefer to keep the original choice, that is $a^*_{13} = a^*_{23}$ (c^*), as the stacking direction. Contrary to the first attempts of Makovicky (in Makovicky & Hyde, 1992), no twinning could be observed in the selected crystal, which simplified the data collection and the structure determination of such a complex crystal structure.

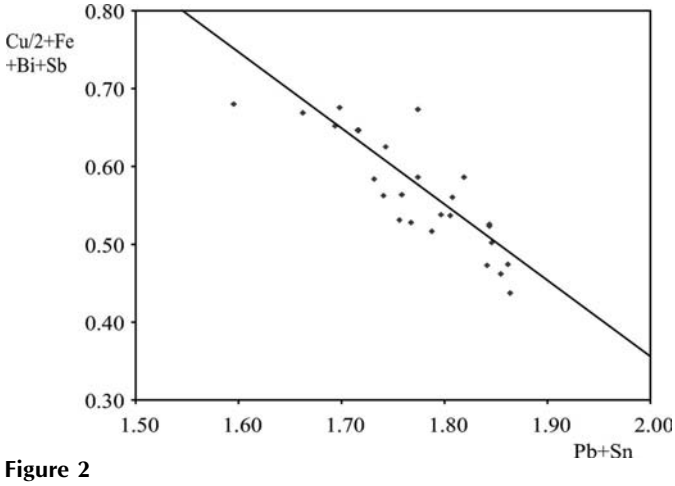

Figure 2
Linear negative correlation between (Cu/2 + Fe + Bi + Sb) and (Pb + Sn) illustrating the double substitution: Pb → (Bi, Sb) and Sn → (Fe, Cu/2) (straight line set with a theoretical gradient of −1). Data from Table 1.

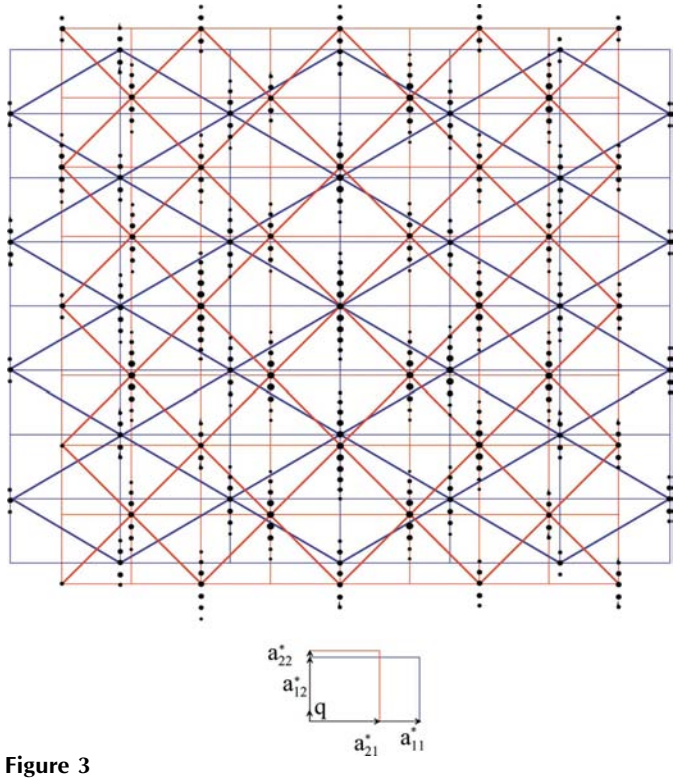

Figure 3
Projection along the (c^*) axis of an idealized diffraction pattern of levyclaudite-(Sb). Thick lines: primitive cells; thin lines: C centered cells. Blue line: H subsystem; red lines: Q subsystem.

The $[Sn_x(Cu_2)_{1-x}]S_2$, or first, subsystem, which will be hereafter considered as the reference subsystem, can be indexed by a triclinic basic primitive cell with a'_{11} = 3.6510 (5), a'_{12} = 3.6514 (5), a'_{13} = 11.9037 (10) Å, α'_1 = 87.572 (9), β'_1 = 88.149 (9), γ'_1 = 60.330 (9)°, V'_1 = 137.75 (2) Å^3 and $\mathbf{q}'_{11}$ = 0.07453 (7)$\mathbf{a}^{*\prime}_{11}$ + 0.07804 (7)$\mathbf{a}^{*\prime}_{12}$ + 0.0135 (3)$\mathbf{a}^{*\prime}_{13}$ (refinement from 3509 reflections with 3067 satellites). Notice that the parameters with a prime superscript refer to the primitive cell (as opposed to those referring to the centred cell, see below). The $(Pb_ySb_{1-y}S)$, or second subsystem (see above), has the dimensions a'_{21} = 4.1316 (3), a'_{22} = 4.1334 (3), a'_{23} = 12.1450 (11) Å, α'_2 = 99.660 (7), β'_2 = 96.455 (6), γ'_2 = 90.427 (6)°, V'_2 = 203.09 (6) Å^3 and $\mathbf{q}'_{21}$ = 0.07345 (7)$\mathbf{a}^{*\prime}_{21}$ − 0.06844 (7)$\mathbf{a}^{*\prime}_{22}$ + 0.0099 (3)$\mathbf{a}^{*\prime}_{23}$ (refinement from 3752 reflections with 3213 satellites). Although both subsystems can be brought to common $a^*_{\nu1}$ and $a^*_{\nu2}$ intralayer directions through centring (see below), the integration and structure determination were initially carried out using primitive cells.

Intensity integration of satellites up to fifth order and a standard Lorentz–polarization correction were performed with the Bruker–Nonius *EvalCCD* program package, both subsystems being considered independently. Subsequent calculations were all carried out with a beta version of the *JANA2006* program suite (Petricek *et al.*, 2006), unless otherwise stated. The two data sets were corrected for absorption by the Gaussian integration method using the crystal shape and dimension previously optimized with *X-shape* (Stoe & Cie, 1996), based on the *Habitus* program (Herrendorf, 1993). The intensities were then adjusted to the same scale, using 1762 common reflections with $I > 10\sigma(I)$, after a correct higher-dimension indexing (see below). Finally, the 99 197 reflections were averaged according to the $\overline{1}$ point group ($R_{\rm int}$ = 0.070) to give a set of 13 027 independent observed reflections at a $2.5\sigma(I)$ level.

3.2. Superspace symmetry

In classical inorganic misfit-layer compounds, one class among all composite structures, two periodic layered structures of different chemical composition stack alternately to yield an intergrowth aperiodic crystal if the two unit cells are mutually incommensurate. A complete description of all the structural features is only possible within the superspace approach (Janner & Janssen, 1980; van Smaalen, 1992, 1995). The diffraction pattern exhibits two sets of strong reflections corresponding to the reciprocal lattices of two basic structures. Satellite reflections are observed, generally weak when they are due to the mutual interaction, but stronger when antiphase boundaries are found [*e.g.* in $(SbS)_{1.15}TiS_2$]. In levyclaudite-(Sb) the satellite intensities are very strong and observable up to high order, in agreement with all previous observations by X-ray or electron diffraction on cylindrite (Makovicky, 1976; Williams & Hyde, 1988; Wang & Kuo, 1991). Such a phenomenon is associated with a very large modulation within each layer, in addition to the weak interaction between the layers.

With one reciprocal axis, $\mathbf{a}^{*\prime}_{13} = \mathbf{a}^{*\prime}_{23}$, and one incommensurate modulation vector, $\mathbf{q}'_{11} = \mathbf{q}'_{21}$, in common, the set of all diffraction peaks of levyclaudite-(Sb) can be indexed with six integer indices. Therefore, the full description can be as much as (3 + 3)-dimensional unless some additional integer relationships exist. As a correct choice of integer-independent basis vectors plays a crucial role in the structure determination, a detailed description follows. To easily understand our setting selection, we have to work momentarily with the $(Pb_ySb_{1-y}S)$ Q subsystem as the reference subsystem (first subsystem, $\nu = 1$), since this was indeed our original choice (at the end of this paragraph we will permute back the two subsystems to follow the usual setting of the classical inorganic misfit-layer compounds for which the NbS_2- or TiS_2-type layer is usually taken as the reference layer). The first three vectors of the full higher-dimension description are chosen as the three reciprocal basis vectors of $(Pb_ySb_{1-y}S)$ (first subsystem, $\nu = 1$): $\mathbf{a}^{*\prime}_i = \mathbf{a}^{*\prime}_{1i}$ for i = 1–3. The fourth vector is taken as the modulation vector: $\mathbf{a}^{*\prime}_4 = \mathbf{q}'_{11}$. For the description of the second subsystem, $[Sn_x(Cu_2)_{1-x}]S_2$, only two vectors remain to be defined since the stacking direction and the modulation vector are common to both subsystems, *i.e.* $\mathbf{a}^{*\prime}_{23} = \mathbf{a}^{*\prime}_3$ and $\mathbf{q}'_{12} = \mathbf{a}^{*\prime}_4$. The fifth vector, which will be the second modulation vector $\mathbf{q}_{12}$ of the first reference subsystem, can then be chosen as $\mathbf{a}^{*\prime}_5 = \mathbf{a}^{*\prime}_{22}$. If this vector selection is complete, it should be possible to express the remaining vector of the second subsystem, $\mathbf{a}'_{21}$, as a linear integer combination of the five already selected vectors. This is indeed the case, with $\mathbf{a}^{*\prime}_{21} = \mathbf{a}^{*\prime}_{11} - \mathbf{a}^{*\prime}_{12} - \mathbf{q}'_{11} - \mathbf{q}'_{12} = \mathbf{a}^{*\prime}_1 - \mathbf{a}^{*\prime}_2 - \mathbf{a}^{*\prime}_4 - \mathbf{a}^{*\prime}_5$, valid within experimental accuracy. Thus, only five reciprocal vectors $\mathbf{M}^{*\prime} = (\mathbf{a}^{*\prime}_{11}, \mathbf{a}^{*\prime}_{12}, \mathbf{a}^{*\prime}_{13}, \mathbf{q}'_{11}, \mathbf{a}^{*\prime}_{22})$ describe the whole diffraction pattern, including satellites. This also means that the modulation effects are induced by the two-dimensional misfit character of the crystal. The second subsystem, reciprocal vectors and $\mathbf{q}$ wavevectors, can be made as the reference subsystem through the application of the $\mathbf{W}^2$ matrix to $\mathbf{M}^{*\prime}$ ($\mathbf{W}^1$ being the unitary matrix; van Smaalen, 1995)

$$\mathbf{W}^2 = \begin{pmatrix} 1 & -1 & 0 & -1 & -1 \\ 0 & 0 & 0 & 0 & 1 \\ 0 & 0 & 1 & 0 & 0 \\ 0 & 0 & 0 & 1 & 0 \\ 1 & 0 & 0 & 0 & 0 \end{pmatrix}.$$

After permuting back the two subsystems so that $[Sn_x(Cu_2)_{1-x}]S_2$ now becomes the reference (first subsystem, $\nu = 1$), the $\mathbf{W}^2$ matrix becomes

$$\mathbf{W}^2 = \begin{pmatrix} 0 & 0 & 0 & 0 & 1 \\ -1 & -1 & 0 & -1 & 1 \\ 0 & 0 & 1 & 0 & 0 \\ 0 & 0 & 0 & 1 & 0 \\ 0 & 1 & 0 & 0 & 0 \end{pmatrix}.$$

Out of the five selected vectors, only three are linearly independent. Therefore, two of them (the modulation vectors of the first subsystem) can be expressed as a linear combination of the first three

$$\begin{pmatrix} \mathbf{q}'_{11} = \mathbf{a}^{*\prime}_4 \\ \mathbf{q}'_{12} = \mathbf{a}^{*\prime}_5 \end{pmatrix} = \sigma' \begin{pmatrix} \mathbf{a}^{*\prime}_1 \\ \mathbf{a}^{*\prime}_2 \\ \mathbf{a}^{*\prime}_3 \end{pmatrix}.$$

The σ' matrix components {$[Sn_x(Cu_2)_{1-x}]S_2$ as the first subsystem} have been determined as

$$\sigma' = \begin{pmatrix} \sigma'_{11} & \sigma'_{12} & \sigma'_{13} \\ \sigma'_{21} & \sigma'_{22} & \sigma'_{23} \end{pmatrix} = \begin{pmatrix} 0.07453\,(7) & 0.07804\,(7) & 0.0135\,(3) \\ 0.22090\,(9) & 0.85286\,(8) & 0.4429\,(3) \end{pmatrix}.$$

Within the primitive cell, with the $[Sn_x(Cu_2)_{1-x}]S_2$ first subsystem as a reference, the possible superspace group is $G_s = P\bar{1}(\sigma'_{11}, \sigma'_{12}, \sigma'_{13}; \sigma'_{21}, \sigma'_{22}, \sigma'_{23})$. This superspace group was confirmed by the structure refinement (see below).

Although this is the setting that was used for the initial structure analysis, it is more convenient, without any loss of information, to describe the structure determination and analyse the atomic arrangement within a non-standard *C*-centred cell. This centred cell was not considered in the initial stage, since it makes the subsystem relationships ($\mathbf{W}^v$ matrix) slightly more complicated. The unit-cell dimension obtained after the *C* centring are for the $[Sn_x(Cu_2)_{1-x}]S_2$ first subsystem: a_{11} = 3.6661 (3), a_{12} = 6.3138 (5), a_{13} = 11.9028 (10) Å, α_1 = 92.490 (7), β_1 = 90.590 (8), γ_1 = 89.986 (8)°, V_1 = 275.25 (7) Å^3, with $\mathbf{q}_{11}$ = 0.00338 (6)$\mathbf{a}^*_{11}$ + 0.15278 (14)$\mathbf{a}^*_{12}$ − 0.0138 (3)$\mathbf{a}^*_{13}$ (refinement from 3562 reflections with 3119 satellites) and for the $(Pb_ySb_{1-y}S)$ second subsystem: a_{21} = 5.8218 (6), a_{22} = 5.8645 (5), a_{23} = 12.1443 (13) Å, α_2 = 92.326 (7), β_2 = 78.533(9), γ_2 = 90.019 (8)°, V_2 = 406.00 (10) Å^3, with $\mathbf{q}_{21}$ = 0.00179 (10)$\mathbf{a}^*_{21}$ + 0.14283 (11)$\mathbf{a}^*_{22}$ − 0.0045 (3)$\mathbf{a}^*_{23}$ (refinement from 3909 reflections with 3371 satellites). It is worth noticing that the common incommensurate $\mathbf{q}$ wavevector is slightly tilted from the $a^*_{11}a^*_{12}$ plane, in agreement with electron microscopy observations (Williams & Hyde, 1988; Wang & Kuo, 1991; Wang & Buseck, 1992).

In this new setting, the components of the σ matrix are

$$\sigma = \begin{pmatrix} \sigma_{11} & \sigma_{12} & \sigma_{13} \\ \sigma_{21} & \sigma_{22} & \sigma_{23} \end{pmatrix} = \begin{pmatrix} 0.00338\,(6) & 0.15278\,(14) & -0.0138\,(3) \\ 0.63105\,(7) & 1.07460\,(17) & -0.4438\,(3) \end{pmatrix}$$

and the $\mathbf{W}^2$ matrix is equal to

$$\mathbf{W}^2 = \begin{pmatrix} 0 & -1 & 0 & -1/2 & 1 \\ 0 & 1 & 0 & 1/2 & 0 \\ 0 & 0 & 1 & 0 & 0 \\ 0 & 0 & 0 & 1 & 0 \\ 1 & 1 & 0 & 0 & 0 \end{pmatrix}.$$

The possible superspace group is then $G_s = C\bar{1}(\sigma_{11}, \sigma_{12}, \sigma_{13}; \sigma_{21}, \sigma_{22}, \sigma_{23})$, confirmed by the structure refinement as already stated.

The direct centred lattices viewed along the common $\mathbf{a}^*_3$ indicated in Fig. 3 are both almost parallel and orthogonal. If the orthogonality condition were exactly fulfilled, it would impose some additional restrictions on the components of the modulation vectors, σ_{ij}. Following the derivation of van Smaalen (1992), the form of the $\mathbf{W}^2$ matrix for the centred cell gives the relations

$$\mathbf{a}_{21} = \frac{1}{\xi}\left[\left(1 + \frac{1}{2}\sigma_{12}\right)\mathbf{a}_{11} - \frac{1}{2}\sigma_{11}\mathbf{a}_{12}\right]$$

$$\mathbf{a}_{22} = \frac{1}{\xi}\left[\left(-\frac{1}{2}\sigma_{11} + \sigma_{21}\right)\mathbf{a}_{12} + \left(1 + \frac{1}{2}\sigma_{12} - \sigma_{22}\right)\mathbf{a}_{11}\right]$$

where $\xi = \sigma_{21} + \frac{1}{2}(\sigma_{21}\sigma_{12} - \sigma_{11}\sigma_{22})$.

From the $\mathbf{a}_{21} \| \mathbf{a}_{11}$ and $\mathbf{a}_{22} \| \mathbf{a}_{12}$ conditions we obtain the restrictions $\sigma_{11} = 0$ and $\sigma_{22} - \sigma_{12}/2 = 1$, respectively. Our experimental results give σ_{11} = 0.00338 (6) and $\sigma_{22} - \sigma_{12}/2$ = 1.07460 − 0.15278 × 0.5 = 0.99821, which are similar to the conditions for parallel cell axes.

3.3. Structure refinement

The structure refinement was initiated from the atomic arrangement found in the inorganic $(MS)_{1+\delta}TS_2$ compounds by replacing *M* by (Pb,Sb) in the Q layer, and *T* by (Sn,Cu_2) in the H layer, with Cu in a triangular coordination on both sides of the $[Sn_x(Cu_2)_{1-x}]S_2$ layer, in replacement of Sn atoms in octahedral coordination in the middle of the layer. It was soon realized that the average structure could not be refined, given the strong observed modulation (satellites up to the fifth order measured for $\mathbf{q}_{11}$). Therefore, Fourier amplitudes of the (1,0) displacive modulation function were immediately introduced in the starting structural model. Simultaneously, the site occupancies Sn and Cu were refined without any restriction and those of Pb and Sb with a full site occupation constraint; a free refinement of the latter atoms on the same position yielded non-physical occupations. The refinement smoothly converged to a rather good *R* value of 0.140 (0.119, 0.131, 0.140, 138, 0.162, 0.224 for zeroth, first, second, third, fourth and fifth order, respectively) for 12 015 reflections and only 48 parameters, demonstrating the quasi-harmonic nature of the $\mathbf{q}_{11}$ modulation wave. Notice that all refinements were carried out with reflections up to $\sin(\theta)/\lambda$ = 0.75 Å^{-1} and at the $2.5\sigma(I)$ level, without including non-observed reflections in the calculations. The reason for the latter choice is the presence of an increasing fraction of unobserved reflections at high scattering angle as the satellite order rises, which adds significant noise to the Fourier synthesis. Sn and Cu site occupancies were found to be in good agreement with the expected $Sn_x(Cu_2)_{1-x}$ relationship and were subsequently constrained to fulfil that relationship. The introduction of anisotropic displacement parameters for all atoms except the S atoms slightly improved the agreement (*R* = 0.129).

At that stage, a search for a possible ordering of both (Pb,Sb) and (Sn,Cu_2) couples was initiated. First, (1,0) occupation modulation amplitudes were introduced for the (Pb,Sb) mixed site with a site occupancy complementarity constraint. A significant improvement was obtained (*R* = 0.116) with a segregation of atoms. The same attempt for the (Sn,Cu_2) couple was not successful, either in the residual *R*-value

Table 3
Residual factors for the (3 + 2)-dimensional superspace refinement of levyclaudite-(Sb).

R factors defined as $R = \Sigma||F_o| - |F_c||/\Sigma|F_o|$ and $wR = [\Sigma w(|F_o| - |F_c|)^2/\Sigma w|F_o|^2]^{1/2}$.

Subsystem (H and Q) and common sets are only subdivisions of the main reflection set.

Reflection subset	No. of reflections (obs)	$R(F)/wR(F)$
All	12 026	0.0741/0.0895
Main	1597	0.0477/0.0698
First order	3257	0.0594/0.0769
Second order	2850	0.0732/0.0909
Third order	2094	0.0895/0.0983
Fourth order	1410	0.120/0.123
Fifth order	818	0.187/0.176
H: $[Sn_x(Cu_2)_{1-x}]S_2$	690	0.0407/0.0601
Q: $(Pb_ySb_{1-y}S)$	894	0.0532/0.0769
Common	13	0.0829/0.104

Table 4
Experimental details for levyclaudite-(Sb).

Crystal data	
Chemical formula	$(Pb_{0.701}Sb_{0.299}S)_{1.357}(Sn_{0.851}Cu_{0.299}S_2)$
M_r	474.1
Cell setting, space group	Triclinic, $C\bar{1}$ (σ_{11}, σ_{12}, σ_{13}; σ_{21}, σ_{22}, σ_{23})
Temperature (K)	293
a_{11}, a_{12}, a_{13} (Å)	3.6661 (3), 6.3138 (5), 11.9028 (5)
α_1, β_1, γ_1 (°)	92.490 (7), 90.590 (8), 89.986 (8)
V_1 (Å^3)	275.25 (7)
Z	2
D_x (Mg m^{-3})	5.709
$\mathbf{q}_{11}$	0.00338 (6)$\mathbf{a}^*_{11}$ + 0.15278 (14)$\mathbf{a}^*_{12}$ − 0.0138 (3)$\mathbf{a}^*_{13}$
$\mathbf{q}_{12}$	0.63105 (7)$\mathbf{a}^*_{11}$ + 1.07460 (17)$\mathbf{a}^*_{12}$ − 0.4438 (3)$\mathbf{a}^*_{13}$
Radiation type	Mo $K\alpha$
μ (mm^{-1})	37.04
Crystal form, colour	Platelet, black
Crystal size (mm)	0.3 × 0.2 × 0.00
Data collection	
Diffractometer	Bruker–Nonius KappaCCD
Monochromator	Oriented graphite (002)
Data collection method	φ/ω scan
Absorption correction	Gaussian
T_{min}	0.039
T_{max}	0.912
No. of measured, independent and observed reflections	99 197, 29 574, 12 012
Criterion for observed reflections	$I > 2.5\sigma(I)$
R_{int}	0.070
$\sin\theta/\lambda_{max}$ (Å^{-1})/θ_{max} (°)	0.807/35.0
Refinement	
Refinement on	F
$R[F^2 > 2\sigma(F^2)]$, $wR(F^2)$, S	0.074, 0.090, 2.65
No. of reflections	12 026
No. of parameters	186
H-atom treatment	No H atoms present
Weighting scheme	Based on measured s.u.'s; $w = 1/[\sigma^2(F) + 0.0004F^2]$
$(\Delta/\sigma)_{max}$	0.001
$\Delta\rho_{max}$, $\Delta\rho_{min}$ (e Å^{-3})	3.34, −3.21

Computer programs used: *JANA2006* (Petricek *et al.*, 2006).

improvement or in the atomic ordering. From this partial solution, the structural model was improved step by step by adding various modulation amplitudes [(1,0), (2,0), (3,0), (4,0), (0,1) and (1,1) harmonics] for site occupancy, displacement and the Debye–Waller factor. At each step of this rather long procedure, the usefulness and validity of the additional parameters was checked through difference-Fourier syntheses and parameter significance. Notice that other harmonics were also considered but not kept in the final model. Special attention was paid to the (0,1) and (1,1) harmonics, which incorporate the layer interactions along the *a* misfit direction and both the *a* and *b* misfit directions, respectively. Indeed, the structure analysis (see below) reveals rather short Pb—Cu distances for some values of the second internal coordinate, t_2, which implies an ordering of (Sn/Cu_2) as a function of t_2 and/or an important displacement of the Pb and Cu atoms. However, without the observation of true satellites for the second wave (*i.e.* $hklmn$, $h \neq 0$ and $n \neq 0$), it was not possible to refine the site occupancy since the harmonics of the occupation modulation functions give a contribution to the intensity of the satellite of the corresponding order only. Only (0,1) and (1,1) displacive modulation functions could be introduced for Pb, which were not sufficient for increasing the short Pb—Cu distances. In the final stage, the refinement converged to R = 0.0741 (wR = 0.0895) for 12 026 independent reflections (2.5σ level) and 186 parameters. The partial residual factors are given in Table 3. Crystal characteristics, data collection and reduction parameters, and refinement results are given in Table 4.[1] Atomic coordinates, occupation parameters, anisotropic displacement parameters and their modulation parameters are given in Tables 5–7.

4. Structure analysis and description

The overall stoichiometry obtained through the lattice parameter refinements (which determines the Q/H ratio) and the structure refinement (which gives the Pb/Sb and Sn/Cu ratios), *i.e.* $(Pb_{0.701}Sb_{0.299}S)_{1.357}(Sn_{0.851}Cu_{0.299}S_2)$, is in reasonable agreement with the formula obtained by the EPM analysis, $(Pb_{0.735}Sb_{0.244}S)_{1.356}[Sn_{0.761}(Cu_2)_{0.200}]S_2$. The charge balance calculated from the refined formula, obtained from the expected $(Pb^{II}_ySb^{III}_{1-y}S^{-II})_{1+\delta}[Sn^{IV}_x(Cu^{I}_2)_{1-x}S^{-II}_2]$ oxidation state attribution, is much closer to neutrality (6.82+/6.71−) than that deduced from the analysis (6.43+/6.71−). A charge transfer of *ca* 0.35 e$^-$ per formula unit from the Q layer to the H layer can be inferred from the refinements, to assure the global charge balance governing the composite structure stability.

The cell parameters of the H layer obtained from the studied levyclaudite-(Sb) crystal are very close to those already reported for levyclaudite (see Tables 2 and 4), in agreement with the similar Cu-for-Sn substitutions (26 and 30%, respectively). It is worth noticing that cylindrite, levyclaudite and levyclaudite-(Sb) show a remarkable homogeneity in their H sub-cell dimensions, despite the Fe-for-Cu_2 substitution. In contrast, the levyclaudite-(Sb) and levyclau-

[1] Supplementary data for this paper are available from the IUCr electronic archives (Reference: CK5020). Services for accessing these data are described at the back of the journal.

Table 5
Fractional atomic coordinates, their Fourier series modulation terms, equivalent isotropic displacement parameters (Å^2) and s.u.s for levyclaudite-(Sb).

The modulation wave for an f position parameter i of an atom μ of a subsystem ν is classically written as

$$f^{\mu}_{\nu i}(x_4, x_5) = f^{\mu}_{\nu i,0} + \sum_{n_1,n_2}^{\infty} f^{\mu}_{i,s,n_1,n_2} \sin[2\pi(n_1 x_{\nu 4} + n_2 x_{\nu 5})] + \sum_{n_1,n_2}^{\infty} f^{\mu}_{i,c,n_1,n_2} \cos[2\pi(n_1 x_{\nu 4} + n_2 x_{\nu 5})].$$

Coordinates of μ of an atom refer to its own subsystem unit cell.

Atom (μ)	ν	Wave	x	y	z	U_{eq}
Sn	1		0	0	0	0.01480 (12)
		s,1,0	−0.00159 (16)	−0.00481 (8)	−0.06455 (5)	
		c,1,0	0	0	0	
		s,2,0	0.00004 (18)	−0.00395 (8)	−0.00108 (5)	
		c,2,0	0	0	0	
		s,3,0	0.0003 (2)	−0.00075 (10)	0.00042 (6)	
		c,3,0	0	0	0	
Cu	1		0.0029 (9)	0.0057 (5)	0.1147 (3)	0.0229 (11)
		s,1,0	−0.0012 (13)	−0.0092 (6)	−0.0611 (4)	
		c,1,0	0.0018 (11)	0.0184 (6)	−0.0013 (4)	
		s,2,0	0.0003 (15)	−0.0036 (7)	0.0014 (4)	
		c,2,0	0.0002 (13)	−0.0021 (7)	−0.0001 (4)	
S1	1		0.5033 (2)	0.84278 (12)	0.12342 (7)	0.0177 (3)
		s,1,0	−0.0012 (4)	−0.00397 (18)	−0.06312 (12)	
		c,1,0	0.0018 (3)	0.02435 (17)	−0.00034 (11)	
		s,2,0	−0.0001 (4)	−0.00411 (19)	−0.00102 (12)	
		c,2,0	−0.0002 (4)	−0.00007 (19)	−0.00031 (11)	
Pb	2		0.05541 (5)	0.24113 (4)	0.36783 (2)	0.03573 (12)
		s,1,0	0.02947 (8)	−0.00518 (7)	−0.07516 (4)	
		c,1,0	−0.00108 (7)	−0.02618 (6)	0.00011 (3)	
		s,0,1	−0.0042 (3)	−0.00529 (17)	0.00240 (9)	
		c,0,1	−0.0036 (3)	−0.00533 (16)	−0.00363 (9)	
		s,2,0	−0.00043 (8)	−0.00055 (7)	−0.00090 (4)	
		c,2,0	0.00007 (8)	−0.00090 (7)	−0.00095 (4)	
		s,3,0	−0.00143 (10)	−0.00018 (8)	0.00267 (4)	
		c,3,0	−0.00031 (10)	0.00122 (8)	0.00004 (4)	
		s,4,0	−0.00043 (15)	0.00106 (10)	0.00015 (6)	
		c,4,0	−0.00129 (15)	−0.00002 (10)	0.00023 (6)	
		s,1,1	0.0022 (3)	−0.00435 (17)	0.00189 (9)	
		c,1,1	−0.0053 (3)	0.00496 (16)	0.00287 (9)	
Sb	2		0.0554	0.2411	0.3678	0.03573 (12)
		s,1,0	0.02947 (8)	−0.00518 (7)	−0.07516 (4)	
		c,1,0	−0.00108 (7)	−0.02618 (6)	0.00011 (3)	
		s,0,1	−0.0042 (3)	−0.00529 (17)	0.00240 (9)	
		c,0,1	−0.0036 (3)	−0.00533 (16)	−0.00363 (9)	
		s,2,0	−0.00043 (8)	−0.00055 (7)	−0.00090 (4)	
		c,2,0	0.00007 (8)	−0.00090 (7)	−0.00095 (4)	
		s,3,0	−0.00143 (10)	−0.00018 (8)	0.00267 (4)	
		c,3,0	−0.00031 (10)	0.00122 (8)	0.00004 (4)	
		s,4,0	−0.00043 (15)	0.00106 (10)	0.00015 (6)	
		c,4,0	−0.00129 (15)	−0.00002 (10)	0.00023 (6)	
		s,1,1	0.0022 (3)	−0.00435 (17)	0.00189 (9)	
		c,1,1	−0.0053 (3)	0.00496 (16)	0.00287 (9)	
S2	2		−0.0402 (3)	0.2583 (2)	0.59639 (13)	0.0310 (4)
		s,1,0	0.0280 (4)	−0.0068 (3)	−0.07151 (17)	
		c,1,0	0.0007 (4)	0.0262 (3)	−0.00002 (18)	
		s,2,0	0.0008 (4)	0.0017 (3)	−0.00096 (17)	
		c,2,0	0.0001 (4)	−0.0007 (3)	−0.00049 (17)	

Table 6
Occupation factors, their Fourier series modulation terms and s.u. values for levyclaudite-(Sb).

The modulation wave for a p occupation parameter i of an atom μ of a subsystem ν is classically written as

$$U^{\mu}_{\nu i}(x_4, x_5) = U^{\mu}_{\nu i,0} + \sum_{n_1,n_2}^{\infty} U^{\mu}_{i,s,n_1,n_2} \sin[2\pi(n_1 x_{\nu 4} + n_2 x_{\nu 5})] + \sum_{n_1,n_2}^{\infty} U^{\mu}_{i,c,n_1,n_2} \cos[2\pi(n_1 x_{\nu 4} + n_2 x_{\nu 5})].$$

Atom (μ)	ν	Wave	p
Sn	1		0.851 (2)
Cu	1		0.149
S1	1		1
Pb	2		0.701 (10)
		s,1,0	0.170 (4)
		c,1,0	−0.002 (6)
		s,0,1	0
		c,0,1	0
		s,2,0	0.002 (4)
		c,2,0	0.026 (5)
		s,3,0	−0.042 (5)
		c,3,0	0.017 (6)
Sb	2		0.299 (10)
		s,1,0	−0.170 (4)
		c,1,0	0.002 (6)
		s,0,1	0
		c,0,1	0
		s,2,0	−0.002 (4)
		c,2,0	−0.026 (5)
		s,3,0	0.042 (5)
		c,3,0	−0.017 (6)
S2	2		1

dite Q-layer cell parameters significantly differ, in both periodicity and angle dimensions (12.14 *versus* 11.84 Å, and 78.5 *versus* 90° for instance), but in an opposite way to the expected trend. Indeed, from a pure cation size point of view, replacement of the majority of Bi (in the natural compound) by pure Sb should contract, and not expand, the unit-cell volume. This could be of course compensated by a lower substitution of Pb by Sb, but that is not the case. The apparent contradiction may be related to the difference in coordination of Bi^{3+} and Sb^{3+}. In complex Pb-(Bi/Sb) sulfides, Bi^{3+} generally adopts a rather symmetric environment (octahedral coordination, with one S apex at a longer distance to accommodate the lone electron pair), while Sb^{3+} gives a quite dissymmetric and distorted environment (dissymmetric square pyramidal coordination, with two additional S atoms at a longer distance) because of a stronger stereochemical activity of its lone electron pair. In levyclaudite-(Sb), if Sb atoms have their pyramidal coordination exclusively with S atoms of the Q layer, their lone electron pairs will be directed towards the H layer. Such an electrostatic repulsion may explain the increase of the stacking vector.

If the strong modulation along the b axis (all references to coordinates hereafter refer to the usual setting used for inorganic misfit-layer compounds and adopted in this structure determination, and not to that proposed in previous reports for the cylindrite–levyclaudite 'isomorphous' series) and if the double incommensurateness is accepted, the structure organization in levyclaudite-(Sb) is not fundamentally different from that observed in the $(MX)_{1+\delta}(TX_2)$ inorganic misfit-layer compounds. Indeed, as in the inorganic misfit-layer

compounds, the *MX* Q layers with a distorted PbS/NaCl-type structure alternate with the TX_2 layers with a CdI_2-type structure (see Fig. 4). The first distinguishing characteristic of the levyclaudite-(Sb) structure and of all cylindrite–levyclaudite related systems is the strong modulation of the layers along one, necessarily common, direction given by the **q** wavevector and hereafter referred to as the longitudinal wave direction (see Fig. 5).

Within the $\mathbf{a}_{22}\|\mathbf{a}_{12}$ approximation (see its validity above), we calculate an a_{12}/a_{22} ratio of $\sim$1.0766, which is close to the $14/13 \simeq 1.0769$ commensurate fraction. This means that a $13a_{12}$ periodicity would be a suitable approximation for a cell match along the modulation direction. Although not directly related in theory, this periodicity is consistent with half the modulation wavevector since $1/13 \simeq 0.0769$ matches the $\sigma_{12}/2 = 0.0764$ component of $\mathbf{q}_{11}$. Therefore, there is a 1:2 relationship between the cell mismatch along the modulation direction and the modulation wavelength, as already reported in the literature (for instance, by Williams & Hyde, 1988).

The second distinguishing characteristic is the double incommensurateness, along both the a_{12} (a_{22}) longitudinal wave direction and the a_{11} (a_{21}) transverse wave direction. This is a specific feature of natural two-dimensional misfits of the cylindrite series, as well as of the hydroxy-sulfides of the valleriite series (Makovicky & Hyde, 1981), and has never been observed, to our knowledge, in purely synthetic inorganic misfit compounds.

4.1. The $Sn_x^{IV}(Cu_2^I)_{1-x}S_2^{-II}$ H layer

Within the $[Sn_x(Cu_2)_{1-x}S_2]$ H layer, Sn atoms and Cu_2 'pairs' occupy octahedral sites (see Fig. 4) and are statistically distributed along both the longitudinal and the transverse wave directions. The disorder along the longitudinal wave direction is ascertained by the structure refinement, but that along the transverse direction is not, since no corresponding satellites could be measured (see §3). Sn atoms, on the inversion centre, occupy the octahedral sites with homogeneous Sn—S distances (2.577 Å on average, see Table 8) which are comparable to those observed for instance in SnS_2 (2.572 Å on average; Pałosz & Salje, 1989). It is remarkable to observe only a small dispersion of the Sn—S distances as a function of the internal t_1 coordinate (Fig. 6*a*), although there is a huge displacement of the atoms perpendicular to the layers (see Fig. 6*a*), a small displacement and almost no displacement along the longitudinal and transverse wave directions, respectively (not shown in Fig. 6*a*). The same remark can be made for Cu atoms, as illustrated by Fig. 6(*b*), which occupy triangular sites on both sides of the H layer (see Fig. 4). The Cu—S1 distances (2.119 Å on average) are typical of the Cu—S distances for copper in triangular coordination as observed in the tetrahedrite $Cu_{10}(Fe,Zn)_2Sb_4S_{13}$ for instance (2.26 Å on average; Peterson & Miller, 1986). The shortest Cu—Cu distances of 2.707 (15) Å, to be compared with Cu—Cu distances down to 2.610 Å in Cu_3BiS_3 (wittichenite – Kocman & Nuffield, 1973), or 2.604 and 2.646 Å in Cu_3SbS_3 (skinnerite – Makovicky & Balić-Žunić, 1995), for which weak bonding interactions have been calculated (Pfitzner, 1994), do not exclude weak d^{10}–d^{10} Cu—Cu interactions.

This statistical long-range distribution of Sn and Cu within the H layer does not rule out some short-distance constraints. For instance, local segregation of Cu atoms in adjacent sites within a single layer would create an excess of negative charges, which could not be balanced by S bonding with adjacent cations from the Q layer. For comparison, in the layered compounds of the MPS_3 type (M = Mn, Fe, Co, Ni and Cd; Ouvrard *et al.*, 1985), topologically similar to the H layer, P pairs are isolated by a crown of six transition metal atoms in octahedral coordination. Nevertheless, owing to the misfit character of the studied structure, it is not possible to introduce such a type of short-distance constraint.

4.2. The $(Pb_y^{II}Sb_{1-y}^{III}S^{-II})$ Q layer

In the second $(Pb_ySb_{1-y}S)$ Q subsystem layer, resembling a slice of an NaCl-type structure, the metal atoms are on the outside of the corrugated layer and may therefore make

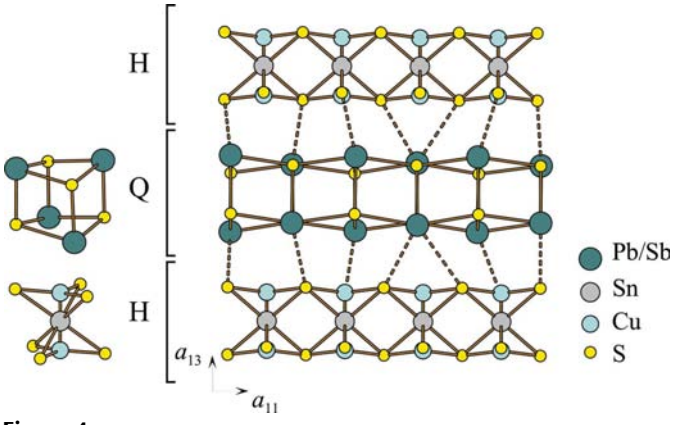

Figure 4
Succession along the a_{13} (a_{23}) axis of the $(Pb_ySb_{1-y}S)$ Q layers with a distorted PbS-/NaCl-type structure and the $[Sn_x(Cu_2)_{1-x}]S_2$ H layers with a 'CdI_2-type' structure. A few unit cells are given along a_{11} to illustrate the incommensurateness. Broken lines indicate the two subsystem interaction.

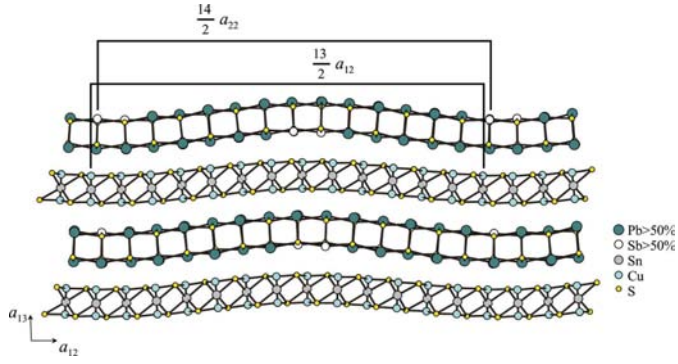

Figure 5
View of several unit cells along the a_{12} axis, close to the modulation direction. Figure limited to approximately one period of the $\mathbf{q}_{11}$ wavevector, that is, one half of the 14/13 cell match approximation. Bonding interaction between the subsystems have been omitted for the sake of clarity. Pb and Sb drawn for site occupancy larger than 0.5.

Table 7
Anisotropic displacement parameters U^{ij} (Å^2), their Fourier series modulation terms and s.u. values for levyclaudite-(Sb).

The modulation wave for a U anisotropic displacement parameter i of an atom μ of a subsystem ν is classically written as

$$U^{\mu}_{\nu i}(x_4, x_5) = U^{\mu}_{\nu i,0} + \sum_{n_1,n_2}^{\infty} U^{\mu}_{i,s,n_1,n_2} \sin[2\pi(n_1 x_{\nu 4} + n_2 x_{\nu 5})] + \sum_{n_1,n_2}^{\infty} U^{\mu}_{i,c,n_1,n_2} \cos[2\pi(n_1 x_{\nu 4} + n_2 x_{\nu 5})].$$

Atom	ν	Wave	U^{11}	U^{22}	U^{33}	U^{12}	U^{13}	U^{23}
Sn	1		0.0137 (2)	0.00983 (16)	0.0208 (3)	−0.00043 (12)	−0.00029 (14)	0.00055 (12)
		s,1,0	0	0	0	0	0	0
		c,1,0	0.0002 (2)	−0.00056 (18)	0.0007 (3)	−0.00012 (17)	0.0002 (2)	−0.00053 (17)
Cu	1		0.0180 (16)	0.0138 (13)	0.037 (2)	−0.0009 (10)	−0.0004 (12)	0.0021 (11)
S1	1		0.0193 (4)	0.0133 (3)	0.0205 (5)	−0.0005 (3)	−0.0005 (3)	0.0008 (3)
Pb	2		0.0382 (2)	0.03020 (16)	0.0390 (2)	−0.00096 (11)	−0.00807 (14)	0.00192 (11)
		s,1,0	−0.0025 (3)	0.0036 (2)	−0.0110 (3)	0.00023 (15)	0.00244(19)	−0.00125 (16)
		c,1,0	0.0002 (3)	0.0007 (2)	0.0019 (3)	−0.00164 (15)	−0.00019 (18)	0.00668 (15)
		s,2,0	0.0006 (3)	0.0008 (2)	0.0009 (3)	0.00069 (16)	−0.0004 (2)	−0.00305 (16)
		c,2,0	−0.0007 (3)	−0.0002 (2)	−0.0007 (3)	−0.00006 (16)	−0.00023 (18)	0.00004 (15)
		s,3,0	−0.0003 (3)	−0.0009 (2)	0.0003 (4)	−0.0002 (2)	0.0016 (3)	0.0007 (2)
		c,3,0	0.0010 (4)	−0.0004 (3)	0.0012 (4)	0.0000 (2)	−0.0008 (3)	0.0000 (2)
Sb	2		0.0382	0.03020	0.0390	−0.00096	−0.00807	0.00192
		s,1,0	−0.0025	0.0036	−0.0110	0.00023	0.00244	−0.00125
		c,1,0	0.0002	0.0007	0.0019	−0.00164	−0.00019	0.00668
		s,2,0	0.0006	0.0008	0.0009	0.00069	−0.0004	−0.00305
		c,2,0	−0.0007	−0.0002	−0.0007	−0.00006	−0.00023	0.00004
		s,3,0	−0.0003	−0.0009	0.0003	−0.0002	0.0016	0.0007
		c,3,0	0.0010	−0.0004	0.0012	0.0000	−0.0008	0.0000
S2	2		0.0395 (8)	0.0295 (6)	0.0237 (7)	−0.0002 (5)	−0.0052 (6)	0.0019 (5)
		s,1,0	0.0098 (11)	0.0059 (8)	−0.0015 (10)	0.0002 (7)	0.0005 (9)	−0.0006 (7)
		c,1,0	0.0006 (11)	0.0016 (8)	−0.0002 (9)	−0.0002 (8)	−0.0003 (8)	0.0015 (7)

possible bonding interactions with the S atoms of the $[Sn_x(Cu_2)_{1-x}S_2]$ H layer. Each metal atom is then coordinated to five S atoms within the $(Pb_ySb_{1-y}S)$ Q layer and to one or two S atoms in the neighbouring $[Sn_x(Cu_2)_{1-x}S_2]$ H layer. The Pb/Sb site occupancy modulation, which could be refined up to third order of the longitudinal $(n_1,0)$ wavefunction, is presented in Fig. 7. It clearly shows a segregation of the elements with Pb preferentially in a domain centered at *ca* t_1 = 0.25 and Sb within the complementary domain centered at *ca* t_1 = 0.75. As can been seen in Fig. 5 from the areas with an Sb site-occupation factor greater than 0.5, for antimony this corresponds to the concave part of the curved layer, at the maximum curvature. By symmetry, this occurs on both sides of the layer. With Sb^{III} smaller in ionic radius than Pb^{II}, this is of course the preferential arrangement as already envisioned by Wang & Kuo (1991) in a tentative model based on an HRTEM study.

This cation ordering within the Q layer is corroborated by the distance analysis. Figs. 8(*a*) and 8(*b*) present t_2 as a function of the second internal coordinate, the Pb/Sb—S and Sb/Pb—S distances at t_1 = 0.25 and t_1 = 0.75, respectively. First, we observed globally longer distances when Pb was preponderant. Then, out of the five intralayer M—S distances, one is significantly shorter [2.780 (6) Å for Pb/Sb—S and 2.641 (6) Å for Sb/Pb—S2, on average], corresponding to the internal bonding perpendicular to the Q layer. If that distance is almost constant [ranging from to 2.755 (6) to 2.807 (6) Å], where Pb occupation is close to 100% (t_1 = 0.25), it oscillates from 2.553 (6) to 2.730 (6) Å where Sb occupation is above 50% (t_1 = 0.75; Fig. 8*c*). Although the Pb/Sb site occupation could not be refined as a modulated function of the second $(0,n_2)$ transverse wave, we can deduce from the distance calculation that Pb and Sb are probably also segregated along the second misfit direction, with Sb preferentially present around t_2 = 0.8 (at t_1 = 0.75). Indeed, at the complementary phase value, t_2 = 0.2 (t_1 = 0.75), the shortest Sb/Pb—S distance [2.730 (6) Å] is close to the Pb/Sb—S distance calculated at t_1 = 0.25 (all t_2 values; see Fig. 8*c*). This analysis on the localization of Sb is corroborated by a study of the valence of (Pb,Sb) as a function of the internal coordinates, which reveals a perfect match of the (Pb,Sb) valence [(Pb,Sb)—S2 bonds] with the shortest (Pb,Sb)—S2 distance, *i.e.* a (Pb,Sb) valence close to 2.0 everywhere except around t_1 = 0.75 and t_2 = 0.8 where it reaches a value of 2.5. By fixing t_2 at the 0.8 value, it is possible to study, as a function of t_1, the M—S distance variation from the Sb-rich part (t_1 = 0.75) of the crystal to a Pb-rich domain (t_1 = 0.25). This is presented in Fig. 9(*a*). We observe that the four remaining M—S intralayer distances are similar and increase as the Sb amount diminishes (from t_1 = 0.75 to t_1 = 0.25), following the trend of the fifth shortest distance.

As already stated, the coordination sphere of Pb and Sb is completed by one or two S atoms in the neighbouring $[Sn_x(Cu_2)_{1-x}S_2]$ H layer. It has been suggested (Wang & Kuo, 1991) that in the cylindrite–levyclaudite compounds the two layers should match to yield an octahedral coordination of the metal atoms; thus the layers curl to compensate for the cell mismatch. Clearly, Fig. 9(*a*) shows the pseudo-octahedral coordination (only one neighbour in the adjacent layer) is realized approximately only in the Sb-rich part of the layer, with an additional neighbouring S atom at *ca* 3.2 Å. When

shifting from the Sb-rich to the Pb-rich domain, a second S atom progressively enters the coordination sphere to finally give a sevenfold coordination. This is in agreement with the greater flexibility of Pb in its geometrical environment. For comparison, van Smaalen *et al.* (1991) described the modulated structure of $(PbS)_{1.18}TiS_2$ by the superspace approach, which detailed the Pb—S interlayer bonding. Coordination evolves from two S at ∼3.30 Å to three S, one closer at ∼3.20 Å with two longer at ∼3.60 Å.

It is interesting to analyse the evolution of the shortest inter-slab Sb/Pb—S distance as a function of the refinement stages. This is reported in Figs. 9(*b*) and 9(*c*) as a function of t_1 (t_2 = 0.8) and t_2 (t_1 = 0.75), respectively. In each stage, the Pb/Sb occupational parameters have been fixed to their final values. In the first stage, only (1,0) harmonics for the *y* and *z* displacive parameters are introduced (for all atoms, as in the final model). Then the (1,0) harmonics for the *x* coordinate are taken into account in a similar way. Subsequently, the (2,0) and (3,0) modulation amplitudes for displacement and the Debye–Waller factor are added. Then, the (0,1) harmonics are introduced for the (Pb,Sb) displacement. Finally the (1,1) harmonics are considered for the same purpose. Clearly, as the structure model improves (each step corresponding to a residual factor lowering) the modulations make the shortest bonds almost constant. This is a normal trend, already observed in inorganic misfit compounds (van Smaalen, 1992, 1995).

Finally, we have seen that it was not possible to observe an ordering between Sn and Cu atoms. However, by calculating the Pb/Sb—Cu distances, too-short distances, as low as

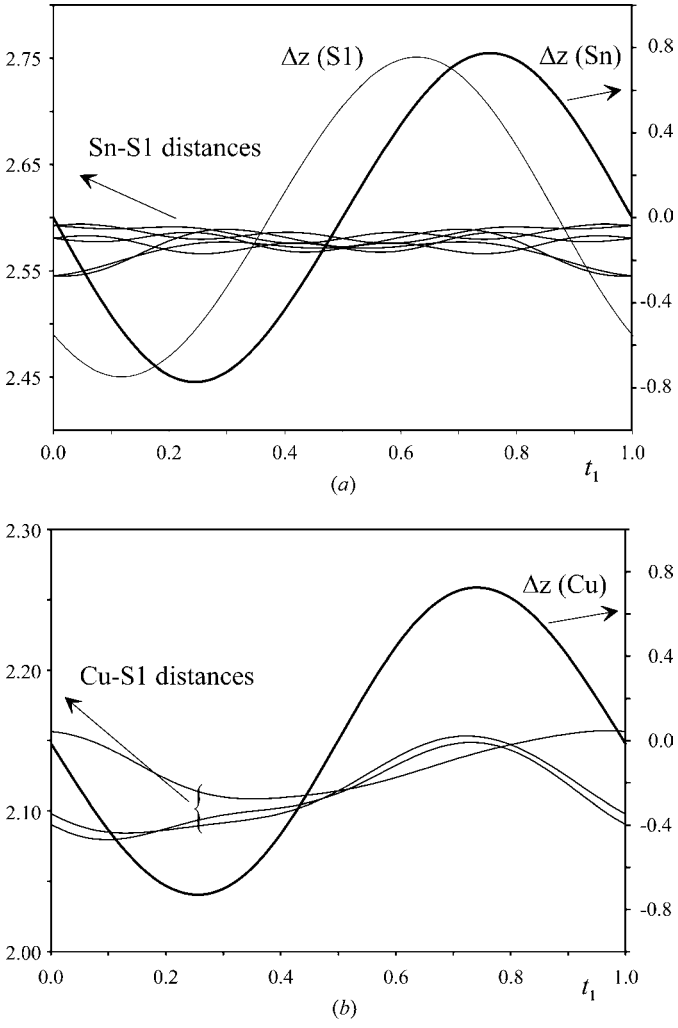

Figure 6
Coordination (distances in Å) and Δz atomic displacement (Å) within the $[Sn_x(Cu_2)_{1-x}]S_2$ H subsystem for (*a*) Sn and S1 and (*b*) Cu atoms.

Table 8
Selected interatomic distances (Å) for levyclaudite-(Sb).

	Basic structure	Average	Min	Max
$[Sn_x(Cu_2)_{1-x}]S$ H subsystem (ν = 1)				
Sn—S1 (×2)	2.5620 (8)	2.569 (3)	2.545 (2)	2.589 (3)
Sn—S1 (×2)	2.5726 (9)	2.576 (3)	2.566 (3)	2.586 (3)
Sn—S1 (×2)	2.5820 (9)	2.586 (3)	2.576 (3)	2.594 (3)
Cu—S1	2.109 (3)	2.110 (10)	2.080 (10)	2.148 (10)
Cu—S1	2.111 (3)	2.113 (10)	2.085 (10)	2.153 (10)
Cu—S1	2.126 (3)	2.133 (9)	2.108 (9)	2.157 (9)
Cu—Cu	2.728 (5)	2.732 (15)	2.707 (15)	2.763 (15)

	Basic structure	Average	Min	Max
$Pb_ySb_{1-y}S$ Q subsystem (ν = 2)				
(Pb,Sb)—S2	2.7180 (15)	2.726 (6)	2.547 (6)	2.824 (6)
(Pb,Sb)—S2	2.9407 (17)	2.941 (8)	2.859 (8)	3.007 (7)
(Pb,Sb)—S2	2.9448 (16)	2.947 (7)	2.865 (7)	3.024 (7)
(Pb,Sb)—S2	2.9506 (14)	2.961 (6)	2.852 (6)	3.132 (5)
(Pb,Sb)—S2	2.9775 (14)	2.995 (6)	2.866 (6)	3.154 (6)

	Min
Subsystem interaction	
(Pb,Sb)—S1	3.123 (5)
(Pb,Sb)—Cu	2.852 (12)
Cu—S2	3.332 (12)

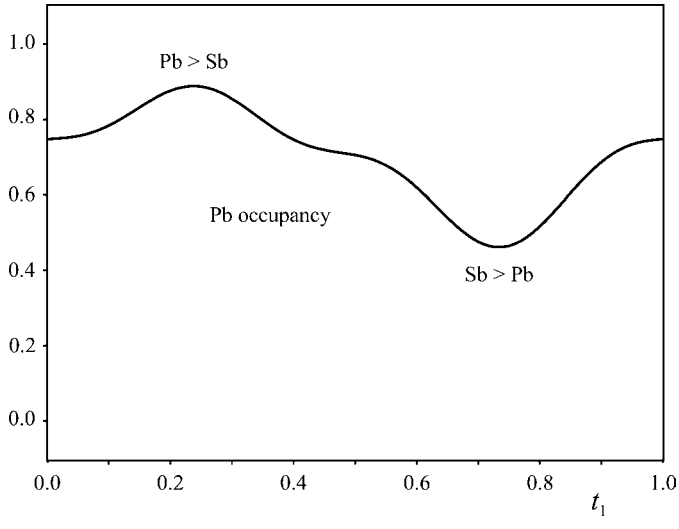

Figure 7
Occupational modulation wave as a function of t_1 for Pb in the $(Pb_ySb_{1-y}S)$ Q subsystem. Full occupancy of the site is assured by a Pb/Sn occupancy complementarity.

2.866 (8) Å, are calculated for some phase domains. Certainly in these regions (zone of longest Pb/Sb—S distances in Fig. 8*c*) there should be a tendency to prefer an Sn occupation to a Cu_2 presence facing the Pb atoms.

5. Discussion

In crystal structures, the modulations observed may have various origins (charge-density wave, occupation *etc.*; van Smaalen, 1995). In two-dimensional misfits, in addition to the

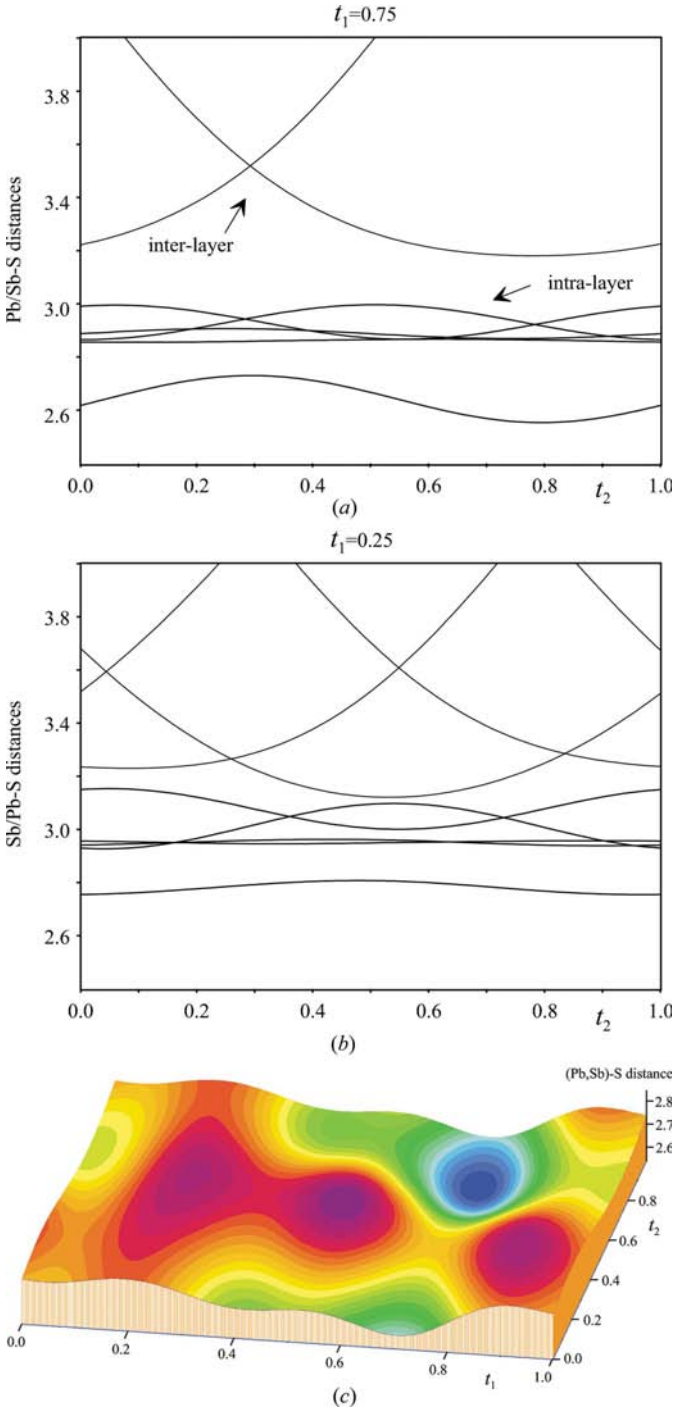

Figure 8
Coordination (distances in Å) as functions of internal t_1 and t_2 coordinates for (Pb,Sb) atoms in the ($Pb_ySb_{1-y}S$) Q subsystem. Shortest intra- and inter-layer (Pb,Sb)—S distances at (*a*) $t_1 = 0.75$ where Sb > Pb and (*b*) $t_1 = 0.25$ for Pb > Sb; (*c*) shortest (Pb,Sb)—S distance as a function of t_1 and t_2.

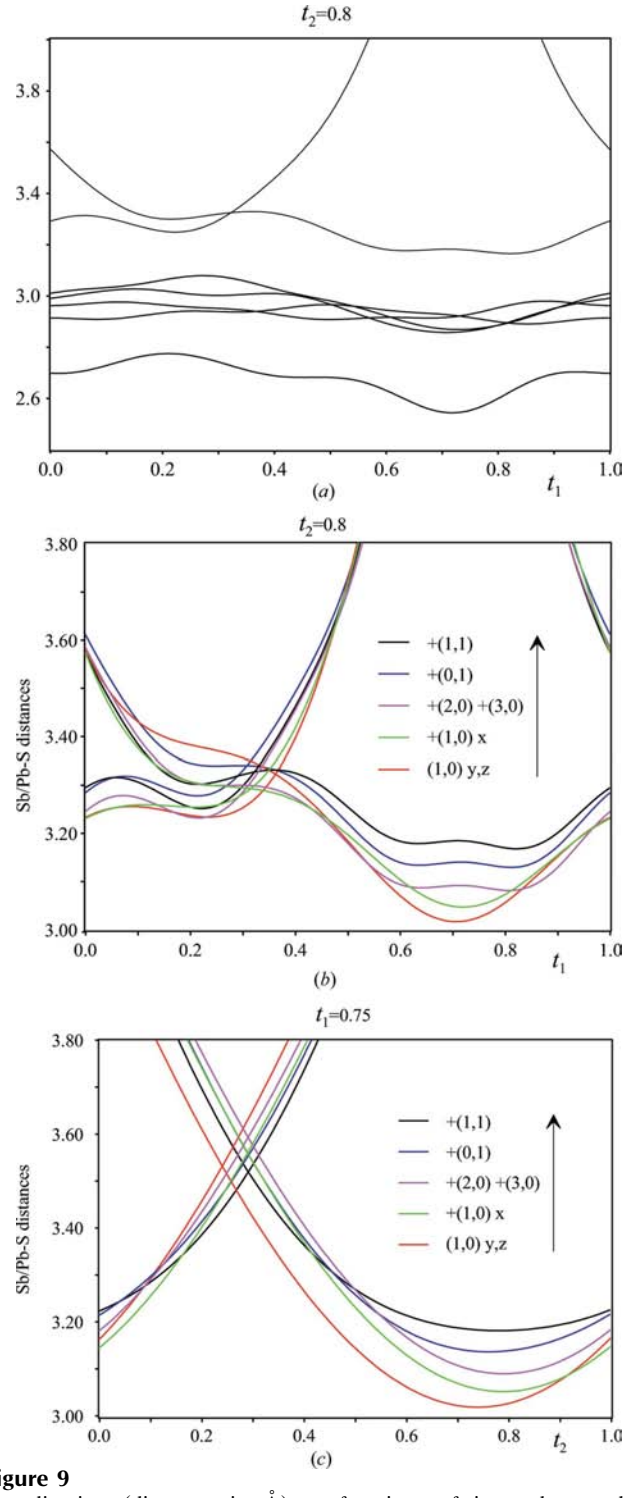

Figure 9
Coordination (distances in Å) as functions of internal t_1 and t_2 coordinates for (Pb,Sb) atoms in the ($Pb_ySb_{1-y}S$) Q subsystem. (*a*) Inter- and intra-layer (Pb,Sb)—S distances for the final structure model ($t_2 = 0.8$); (*b*) and (*c*) evolution of the inter-layer (Pb,Sb)—S1 distance as a function of the refinement stages (see text).

subsystem interaction, two types of modulation have been encountered within a layer, corresponding to displacive and/or occupational modulations. The first type is found in synthetic misfits, within the H layer, where the metal position may be modulated along the misfit direction, in relation to the metal–metal bonding clustering. An example is given by the isotypic crystal structures of $(La_{0.95}Se)_{1.21}VSe_2$ (Ren *et al.*, 1996) and $(LaS)_{1.196}VS_2$ (Cario *et al.*, 2005), where the V—V distance oscillates between and 3.05 and 3.71 Å. The second type is observed in the cylindrite–levyclaudite series where the metal position oscillates orthogonally to the modulation direction (here the semi-commensurate direction), creating the wavy geometry. For our purpose and as a didactical example, this undulation type of modulation will be called 'mondulation' to distinguish it from the inter-layer interaction modulation along the transverse direction.

In cylindrite, such a mondulation appeared in the first structural scheme proposed by Makovicky (1974) for the H layer, but was not clearly observed for the Q layer (initially given as 'T'). The HRTEM study of Williams & Hyde (1988) revealed the strong general mondulation of the cylindrite structure, also visible in the franckeite higher homologue. The similar study of Wang & Kuo (1991) confirmed these two observations. Such a mondulation is also clearly visible in the natural two-dimensional misfit lengenbachite (Williams & Pring, 1988), $Pb_6As_4(Ag,Cu)_2S_{13}$, also through HRTEM imaging. To pinpoint the crystal chemical factors which govern the mondulation, one needs to answer two questions: first, what factor induces the layer undulation, and, secondly, what factor controls its modulation, that is, its long-distance regularity?

5.1. Origin of the undulation in natural two-dimensional misfits

In the structural scheme of Makovicky (1974) for cylindrite, the undulation, only clearly visible in the H layer, is explained by the short-range ordering of the cations (Sn, Sb and Fe) of different sizes and with different geometry. In contrast, Wang & Kuo (1991) pointed to the ordering of Sb *versus* Pb in the Q layer. The present study on levyclaudite-(Sb) proves the validity of the latter model, which is reinforced by the apparent absence of (Cu_2) *versus* Sn ordering within the H layer [*NB* this explanation which is valuable for levyclaudite-(Sb) does not absolutely exclude the complementary role of the H layer in cylindrite as proposed by Makovicky (1974)]. Wang & Kuo (1991) proposed a similar model for franckeite, but with Sb atoms in the two external atom layers of the Q layer (four atoms thick), while Lafond *et al.* (1997) proved, on the contrary, the selective distribution of the Sb atoms exclusively in the two inner atom layers in their crystal structure resolution of an 'Nb-franckeite', $[(Pb,Sb)S]_{2.28}NbS_2$. Williams & Pring (1988) did not propose any explanation for the observed undulation of lengenbachite and their structural scheme concerning the H layer is strongly debatable (Makovicky *et al.*, 1994). As a first conclusion, it appears that, in natural two-dimensional misfits, crystallographic data have so far been very heterogeneous and generally incomplete, and that crystal structure studies based on a superspace approach are a prerequisite to the problem of structural undulation within these compounds.

5.2. Wavelength control

The question of the long-distance regularity, *i.e.* wavelength control, must be related to the question of semi-commensurability along the mondulation direction. Indeed, Makovicky & Hyde (1992) have indicated that, along that direction, the Q and H parameters are more often in the ratio of two successive integers, $(n + 1)\, b_Q$ matching $n\, b_H$ (new cell setting), according to the vernier principle, as shown by various matches compiled from previous studies. For instance, in cylindrite, Makovicky (1976) gave the 13Q/12H match, but synthetic Fe, Zn or Cd derivatives gave matches between 11/10 and 14/13 (Williams, in Makovicky & Hyde, 1992). For franckeite, depending upon the Sn^{2+} for Pb substitution, the match varies from 12Q/11H for the Sn^{2+}-richest member ('incaite' – same author) up to 16Q/15H for the Sn^{2+}-free member ('potosiite' – Wolf *et al.*, 1981). The latter example illustrates the logical increase of n with the increase of the Q sub-cell dimension, that is, the mean size of its constitutive cations (the H layer is assumed to be chemically unchanged, as a first approximation). As already mentioned, the larger Q unit cell of levyclaudite-(Sb) relative to that of natural levyclaudite is also in accordance with a higher vernier ratio (14/13 against 13/12; see Table 2).

The vernier principle also applies to other natural two-dimensional misfit chalcogenides. In lengenbachite, one has a 12Q/11H match (Williams & Pring, 1988). In cannizzarite, $Pb_8Bi_{10}S_{23}$, two matches, 12Q/7H and 17Q/10H, or their combinations, have been described (Makovicky & Hyde, 1992) since the primitive study of Matzat (1979). When the studied material is chemically heterogeneous, the nanometric (sub-crystal) scale studies revealed (crystal) sub-domains with distinct vernier ratios. An AFM–STM (atomic force microscopy–scanning tunneling microscopy) study of franckeite allowed Henriksen *et al.* (2002) to distinguish various areas with vernier ratios of 13/12, 14/13, 15/14 and 16/15 in natural franckeite from Bolivia, which may present variable Sn^{2+} for Pb^{2+} substitution in the Q layer.

All these data clearly demonstrate that the semi-commensurability according to the vernier principle corresponds to a mutual adjustment of the two Q and H layers. Owing to the various solid solutions observed within one structural type, the ratio of the intra-layer unit surfaces of its two constitutive cells necessarily varies continuously. However, for a given chemical composition, there is some degree of elasticity of each cell (as illustrated by the variations of the intra-layer parameter ratio), as well as some degree of flexibility (as illustrated by the variable coordination in the bonding of the Q cation with the S atoms of the H layer), which can adjust the chemistry to a specific semi-commensurate match.

In natural two-dimensional misfits with only one direction of incommensurability (lengenbachite and cannizzarite), this hypothesis of inter-layer adjustment towards semi-commen-

surability seems the only way to control the wavelength. Strong chemical changes during crystal growth adapt the Q/H interface through different successive vernier ratios. In the cylindrite series, the problem is complicated by the frequent observation of a small relative rotation between the Q and H layers, so the mondulation direction deviates from the two related parameters (Makovicky & Hyde, 1992; Wang & Kuo, 1991). Together with the elasticity and flexibility already mentioned, the relative rotation constitutes a third degree of liberty in the mutual adjustment of the two constitutive layers.

In the large field of phyllosilicates, among modulated (commensurate) structures some minerals exist which present a regular mondulation of their constitutive octahedral layer, as suggested by Makovicky & Hyde (1992). The most interesting example is that of the antigorite homologous series, according to the study of Capitani & Mellini (2004). This series has the general formula $M_{3(m-1)}T_{2m}O_{5m}(OH)_{4m-6}$ (M and T: cations with octahedral and tetrahedral coordination, respectively). Along the modulation direction, the m tetrahedra match the $(m-1)$ octahedra. Thus, despite the fact that the alternate up-and-down bonding to the octahedral layer of the tetrahedron sequences would appear to be sufficient to reduce the strain given by the relative sizes of the M and T polyhedra, the modulation also obeys the vernier principle (m = 14–19).

For the m = 17 homologue, the amplitude of the mondulation is 1.286 Å, with a wavelength of a = 43.505 Å (Capitani & Mellini, 2004). For the m = 14 homologue, these values are 1.644 and 35.02 Å, respectively (Dodony *et al.*, 2002). These values are to be compared with values of ∼1.5 and ∼41.0 Å for the H layer of levyclaudite-(Sb).

5.3. Beneath the inter-layer geometrical adjustment; the question of a charge-transfer density modulation wave

The cation heterogeneity inside the two layers (Pb^{2+} *versus* Sb^{3+} in Q; Sn^{4+} *versus* Cu_2^+ in H) superimposes onto the mechanism of the geometrical adjustment of the interface through the problem of charge transfer. This charge transfer (that is, the problem of the charge neutrality) would, on the one hand, impose a local ordering of the four cations while, on the other hand, the interface incommensurability opposes that trend. The modulation wave, expressed in the cylindrite series by the mondulation, represents an equilibrium point between these two opposite trends. In other words, we can refer to a *charge transfer density modulation wave*, which represents a short-range ordering, as illustrated by the question of semi-commensurability, for an energy minimization of this type of composite crystal structure.

In pure synthetic two-dimensional misfits, despite initial appearances, there is always (at least) one of the two layers that presents its own valence modulation, which acts on the charge transfer and then governs the charge-transfer density modulation wave. Some examples are

(i) in $(LaS)_{1.196}VS_2$ (Cario *et al.*, 2005), the V—V modulation corresponds to a modulation of the formal valence of V atoms;

(ii) in $(Gd_{1.18}\square_{0.11}S_{1.27})CrS_2$ (□ = vacancy – Rouxel *et al.*, 1994), the presence of vacancies in the Q layer creates a local deficit of positive charges;

(iii) in $(La_{0.95}Se)_{1.21}VSe_2$ (Ren *et al.*, 1996), the two preceding mechanisms are combined;

(iv) in misfits of the '$[(Pb,Sn)S]_{1+x}$·$[(Nb,Ti)S_2]_m$'-type, chemical analyses have revealed an 'Nb/Ti excess', which corresponds to a partial replacement of Pb by Nb or Ti within the Q layer (Moëlo *et al.*, 1995), inducing a local excess of positive charges.

In the latter example, the relationship between the (Nb,Ti) for (Pb,Sn) substitution and the semi-commensurability was emphasized ('cationic coupling').

Unlike the classic phenomenon of the charge-density wave, this model of the charge-transfer density modulation wave, which is two-dimensional, does not correspond by itself to an electron delocalization, but it may be correlated to such an electron delocalization within the H layer [for instance in $(LaS)_{1.196}VS_2$ cited above].

6. Concluding remarks

Our structure determination of levyclaudite-(Sb) from single-crystal X-ray diffraction constitutes the first (3 + 2)-dimensional superspace approach to a structure of a member of the cylindrite-type minerals. It has shown several crystallographic key features. First, the diffraction pattern of levyclaudite-(Sb) could be interpreted as the combination of two heavily modulated triclinic subsystems with a common **q** wavevector and only one shared reciprocal axis, that is, with a new unpredicted lattice arrangement. The structure of levyclaudite-(Sb) was then shown to be fundamentally not too different from the structures observed for the $(MX)_{1+\delta}(TX_2)$ inorganic misfit-layer compounds, but nevertheless to differ from them by a specific characteristic, that is, a strong modulation of the layers which can be referred to as a mondulation. The distribution of the cations within the two subsystems has been thoroughly studied. If no ordering of Sn and Cu could be observed within the H layer, a segregation of Pb and Sb has, however, been shown with Sb preferentially occupying the inner side of the Q curved layer, at the maximum of curvature.

The local ordering of the Sb trivalent cation in the Q layer is apparently the key to the control of the mondulation. Such a local ordering could not be ultimately resolved in our X-ray single-crystal diffraction study, although it appeared essential to decrypt the general organization of such a complex two-dimensional misfit structure. New analysis with better measurements of the satellite intensities could improve the structure model. For the near future, two approaches must be used as a priority, as exemplified by some recent studies. First, X-ray absorption spectroscopy (XANES and EXAFS) combined with HRTEM should allow the precise coordination of the different cations to be determined and help the elaboration of a more precise structural model. An example of the application of this approach for a two-dimensional misfit compound has been recently published by Leynaud *et al.*

(2003) on $[Sr(Fe_{0.77}Nb_{0.23})_{0.5}S_{1.5}]_{1.13}NbS_2$. Secondly, a more efficient way to analyse the local distribution of Sb within the Q layer is the atomic scale observation of cleavage surfaces by STM and AFM, as exemplified by the study of 'franckeite-Nb' (Bengel *et al.*, 2000).

Whatever the choice of the analysis method, a precise chemical synthesis of such two-dimensional misfits in strictly controlled conditions (chemistry; crystallization in near-equilibrium conditions), in order to obtain well ordered crystals with stable mondulation, is a prerequisite to any study. Numerous experimental studies have been performed up to now, which prove the easy synthesis in the cylindrite family (cylindrite, levyclaudite, franckeite and pure synthetic poles; Nekrasov & Bortnikov, 1975; Sachdev & Chang, 1975; Li, 1984, 1986; Maurel *et al.*, 1990; Crawford, 2002; Bente *et al.*, 2005). More generally, there is still a large field of research on the understanding of the crystal chemistry of two-dimensional misfit chalcogenides in relation to their physical properties (Salyer & Haar, 1997, 2000). The recent study of Cario *et al.* (2006), revealing a dielectric breakdown and a current switching effect in the $(LaS)_{1.196}VS_2$ compound, subordinated to the H layer, is a remarkable example of original physical properties in a two-dimensional misfit. As pointed out by these authors, the presence of a coupled cationic substitution within the Q layer (presence of vacancies or divalent metal) in isotypic derivatives drastically changes their physical properties.

Vaclav Petricek could participate on this work thanks to the support from the Grant Agency of the Czech Republic, grant 202/06/0757.

References

Bengel, H., Jobic, S., Moëlo, Y., Lafond, A., Rouxel, J., Seo, D.-K. & Whangbo, M.-H. (2000). *J. Solid State Chem.* **149**, 370–377.

Bente, K., Wagner, G., Heuer, M., Schorr, S., Krutova, G. N., Doring, T., Oppermann, D. & Kaden, R. (2005). *First Vienna International Conference on Micro- and Nano-Technology*, pp. 249–258. Vienna, Austria

Capitani, G. & Mellini, M. (2004). *Am. Mineral.* **89**, 147–158.

Cario, L., Corraze, B., Meerschaut, A. & Chauvet, O. (2006). *Phys. Rev. B*, **73**, 155116.

Cario, L., Meerschaut, A., Corraze, B. & Chauvet, O. (2005). *Mater. Res. Bull.* **40**, 125–133.

Crawford, G. M. (2002). PhD thesis, University of Texas, El Paso, USA, p. 176.

Dodony, I., Posfai, M. & Buseck, P. R. (2002). *Am. Mineral.* **87**, 1443–1457.

Frenzel, A. (1893). *Neues Jahrb. Miner. Geol. Paleönt.* **2**, 125–128.

Graham, A. R., Thompson, R. M. & Berry, L. G. (1953). *Am. Mineral.* **38**, 536–544.

Henriksen, R. B., Makovicky, E., Stipp, S. L. S., Nissen, C. & Eggleston, C. M. (2002). *Am. Mineral.* **87**, 1273–1278.

Herrendorf, W. (1993). *Habitus.* PhD dissertation, University of Karlsruhe, Germany.

Janner, A. & Janssen, T. (1980). *Acta Cryst.* A**36**, 408–415.

Kocman, V. & Nuffield, E. W. (1973). *Acta Cryst.* B**29**, 2528–2535.

Lafond, A., Nader, A., Moëlo, Y., Meerschaut, A., Briggs, A., Perrin, S., Monceau, P. & Rouxel, J. (1997). *J. Alloys Compd*, **261**, 114–122.

Lambert, S., Leligny, H. & Grebille, D. (2001). *J. Solid State Chem.* **160**, 322–331.

Leligny, H., Grebille, D., Perez, O., Masset, A. C., Hervieu, M., Michel, C. & Raveau, B. (1999). *C. R. Acad. Sci. Paris Ser. IIc Chim.* **2**, 409–414.

Leynaud, O., Caldès, M. T., Guillot-Deudon, C., Ouvrard, G., Lafond, L. & Meerschaut, A. (2003). *Chem. Mater.* **15**, 3753–3758.

Li, J. (1984). *Neues Jahrb. Miner. Abh.* **150**, 45–50.

Li, J. (1986). *Neues Jahrb. Miner. Abh.* **153**, 283–285.

Makovicky, E. (1971). *Am. Mineral.* **56**, 353.

Makovicky, E. (1974*a*). *Neues Jahrb. Miner. Monatsh.* pp. 235–256.

Makovicky, E. (1974*b*). *Fortschr. Miner.* **52**, 49–52.

Makovicky, E. (1976). *Neues Jahrb. Miner. Abh.* **126**, 304–326.

Makovicky, E. & Balić-Žunić, T. (1995). *Can. Mineral.* **33**, 655–663.

Makovicky, E. & Hyde, B. G. (1981). *Struct. Bond.* **46**, 101–170.

Makovicky, E. & Hyde, B. G. (1992). *Mater. Sci. Forum*, **100/101**, 1–100.

Makovicky, E., Leonardsen, E. & Moëlo, Y. (1994). *Neues Jahrb. Miner. Monatsh.* **H.2**, 169–191.

Matzat, E. (1979). *Acta Cryst.* B**35**, 133–136.

Maurel, C., Makovicky, E., Moëlo, Y. & Karup-Møller, S. (1990). SFMC Meeting, Rennes, 5–7 September (abstract).

Meerschaut, A. (1992). *Mater. Sci. Forum*, **100/101**, 414.

Meerschaut, A., Moëlo, Y., Cario, L., Lafond, A. & Deudon, C. (2000). *Mol. Cryst. Liq. Cryst.* **341**, 1–8.

Moëlo, Y., Makovicky, E., Karup-Møller, S., Cervelle, B. & Maurel, C. (1990). *Eur. J. Mineral.* **2**, 711–723.

Moëlo, Y., Meerschaut, A., Rouxel, J. & Auriel, C. (1995). *Chem. Mater.* **7**, 1759–1771.

Nekrasov, I. Ya. & Bortnikov, N. S. (1975) *Metallization Associated with Acid Magmatism*, Vol. I, pp. 280–283. Prague: John Wiley & Sons.

Ouvrard, G., Brec, R. & Rouxel, J. (1985). *Mater. Res. Bull.* **20**, 1181–1189.

Pałosz, B. & Salje, E. (1989). *J. Appl. Cryst.* **22**, 622–623.

Peterson, R. C. & Miller, I. (1986). *Mineral. Mag.* **50**, 717–721.

Petricek, V., Dusek, M. & Palatinus, L. (2006). *JANA2006*, beta version. Institute of Physics, Academy of Sciences of the Czech Republic, Prague, Czech Republic.

Pfitzner, A. (1994). *Z. Anorg. Allg. Chem.* **620**, 1992–1997.

Ren, Y., Baas, J., Meetsma, A., de Boer, J. L. & Wiegers, G. A. (1996). *Acta Cryst.* B**52**, 398–405.

Ren, Y., Meetsma, A., Petricek, V., van Smaalen, S. & Wiegers, G. A. (1995). *Acta Cryst.* B**51**, 275–287.

Rouxel, J., Moëlo, Y., Lafond, A., DiSalvo, F. J., Meerschaut, A. & Roesky, R. (1994). *Inorg. Chem.* **33**, 3358–3363.

Sachdev, S. C. & Chang, L. L. Y. (1975). *Econ. Geol.* **70**, 1111–1122.

Salyer, P. A. & ter Haar, L. W. (1997). *J. Appl. Phys.* **81**, 5163–5165.

Salyer, P. A. & ter Haar, L. W. (2000). *J. Appl. Phys.* **87**, 6025–6027.

Smaalen, S. van (1992). *Mater. Sci. Forum*, **100/101**, 173–222.

Smaalen, S. van (1995). *Cryst. Rev.* **4**, 79–202.

Smaalen, S. van, Meetsma, A., Wiegers, G. A. & de Boer, J. L. (1991). *Acta Cryst.* B**47**, 314–325.

Stoe & Cie (1996). *X-shape*, Version 1.02. Stoe & Cie, Darmstadt, Germany.

Wang, S. & Buseck, P. R. (1992). *Am. Mineral.* **77**, 758–764.

Wang, S. & Kuo, K. H. (1991). *Acta Cryst.* A**47**, 381–392.

Wiegers, G. A. & Meerschaut, A. (1992). *Mater. Sci. Forum*, **100/101**, 101–172.

Wiegers, G. A., Meetsma, A., van Smaalen, S., Haange, R. J. & de Boer, J. L. (1990). *Solid State Commun.* **75**, 689–692.

Williams, T. B. & Hyde, B. G. (1988). *Phys. Chem. Miner.* **15**, 521–544.

Williams, T. B. & Pring, A. (1988). *Am. Mineral.* **73**, 1426–1433.

Wolf, M., Hunger, H.-J. & Bewilogua, K. (1981). *Freib. Forsch. C*, **364**, 113–133.

Zambonini, F., De Fiore, O. & Carobbi, G. (1925). *R. Acad. Sci. Fis. Nat. Napoli*, **31**, 24–29.